Silicon Photonic DWDM Micro-Resonator Link Initialization Under Fabrication Variation

JAMES ROBINSON,[1,*] ROBERT PARSONS,[1] YUYANG WANG,[1] KAYLX JANG,[1] XIANG MENG,[1] AND KEREN BERGMAN[1]

[1]*Department of Electrical Engineering*
Columbia University in the City of New York, New York, 10027, USA
[*]*james.robinson@columbia.edu*

Abstract: Silicon photonic dense wavelength-division multiplexing (DWDM) links based on microresonators are a leading candidate for scaling optical interconnects in high-performance computing. However, fabrication-induced variations in resonant frequencies, free spectral ranges (FSRs), and thermal tuning efficiencies necessitate robust initialization strategies to align resonators with multi-wavelength laser sources. While many prior studies examine individual devices, comprehensive wafer-scale statistical analyses—and their implications for initialization algorithms remain scarce. Here, we report measurements from more than 4,600 fabricated resonators, including microdisks, tapered hybrid-bend (THB) racetracks, and microrings, fabricated on 300-mm wafers. We show that microrings exhibit the largest variation, while microdisks are significantly more uniform. Using these distributions, we evaluate initialization performance through Monte Carlo simulations of two widely used algorithms: barrel-shifting and global-search. Our results establish a clear tradeoff: barrel-shifting offers sub-millisecond initialization with modest power budgets for low-variation devices (e.g. microdisks), whereas global search, though approximately 300 times slower, achieves substantially lower power consumption for high-variation devices (e.g. microrings). This work provides the first wafer-scale statistical framework linking resonator variability to initialization outcomes, and offers practical design guidance for selecting initialization strategies that balance speed, power, and robustness.

1. Introduction

Silicon photonic interconnects have advanced rapidly over the past two decades, offering scalable solutions to the bandwidth and energy constraints of modern high-performance computing (HPC) systems [1–3]. Among the most promising architectures are dense wavelength-division multiplexing (DWDM) links, which employ large buses of resonators—microrings, racetracks, and more recently microdisks—to interface with multi-wavelength laser sources [4–6]. Despite the promise of high density and low power, a fundamental challenge persists: fabrication-induced variations in resonant frequency, FSR, and thermal tuning efficiency disrupt the frequency alignment between resonators and lasers, necessitating thermal initialization schemes [7, 8].

Prior work has explored tuning methods and device demonstrations [9, 10], but two critical gaps remain. First, statistical characterization of variation across large wafer populations is limited, particularly for foundry-scale fabrication. Without such statistics, system designers lack a quantitative foundation for anticipating yield and power budgets. Second, while several initialization algorithms have been proposed, there is less guidance on how device-level variability dictates the appropriate choice of algorithm. For instance, fast initialization is crucial in reconfigurable datacenter settings, while low steady-state power is essential for energy-efficient transceivers, yet these goals are often in tension.

In this work, we address both gaps by presenting the first wafer-scale statistical analysis of over 4,600 fabricated resonators, covering microdisks, THB racetracks, and microrings, and integrating these results into Monte Carlo models of two widely used initialization algorithms: barrel-shifting and global-search. We reveal that the performance and suitability of these

algorithms depend critically on the degree of fabrication variation. Microdisks, with narrow distributions, can be rapidly and efficiently initialized using barrel-shifting, while microrings require the more computationally intensive global-search to achieve acceptable power budgets. Our findings establish a design framework that links measured variation statistics to system-level initialization tradeoffs in speed, power, and yield, guiding the deployment of DWDM silicon photonic links in practical computing environments.

This paper is organized as follows: Section 2 provides an overview of the devices and link examined by our Monte Carlo simulations, including devices such as microdisks and microrings, and the DWDM link architecture. Section 3 discusses the measured statistics of the resonant frequencies of each type of resonator. Section 4 describes our implementation of two initialization algorithms and the results of the Monte Carlo model, which characterizes their power budget sensitivity with respect to component variation. Section 5 discusses the general time-dependent behavior of these algorithms. Section 6 analyzes these results and discusses crucial considerations in algorithm selection, such as device variation, power, and initialization time.

2. Device and Link Architecture

Although existing literature addresses the topic in detail [4, 11–13], we provide a brief overview of the devices and architecture. Here, we focus our discussion on buses of microdisk, microring, and THB racetrack resonators for DWDM interconnects.

2.1. Operational Detuning in the DWDM Link Architecture

DWDM links, exemplified schematically in Fig. 1a, typically rely on high channel counts and modest channel data rates to reduce complexity of the RF driver and receiver circuitry, and hence achieve low power consumption. In DWDM links, the total channel counts are 16, 32, or even more, with an individual data rate of $8 \sim 32$ Gbps [4]. The laser frequencies for each channel are evenly spaced, generated by a comb laser such as a Kerr comb [14], at which frequencies microresonators are pre-designed to resonate. However, even minor fabrication imperfections can easily change the resonant frequency of the resonators by enough to limit modulation depth or render the device totally non-functional [15–17]. To address this issue, thermal initialization is usually used to realign the resonant frequencies [18–20]. We highlight that thermal tuning is directional (red shift in spectrum), as heating increases the effective indices of silicon waveguides. As such, even a minor temperature change that requires a blue shift necessitates a re-initialization of the entire link. Therefore, the designed resonances regularly have intentionally higher frequencies than the intended operating laser frequency. Such design detuning reduces the likelihood of a required blue shift of resonance with respect to the laser frequency, which improves the initialization performance.

In addition, an additional operational detuning offers resilience against potential temperature fluctuations by initially tuning to a frequency blue shifted from the target laser wavelength, providing a small frequency operating window to accommodate environmental temperature fluctuations. This robustness to temperature fluctuation is acquired at the cost of slightly higher power consumption, which should be taken into consideration during the link design. Our models generally assume an operational detuning of 50 GHz, which allows for a operating window of approximately 0.4 nm in the wavelength range of telecommunication C-band based off the resonant frequency temperature dependance measured in [21]. For silicon photonics, this corresponds to a thermal operating window of approximately 5.3 °C, a safe value for most applications. We note that future research may reduce the required thermal window and save additional power consumption according to the applications.

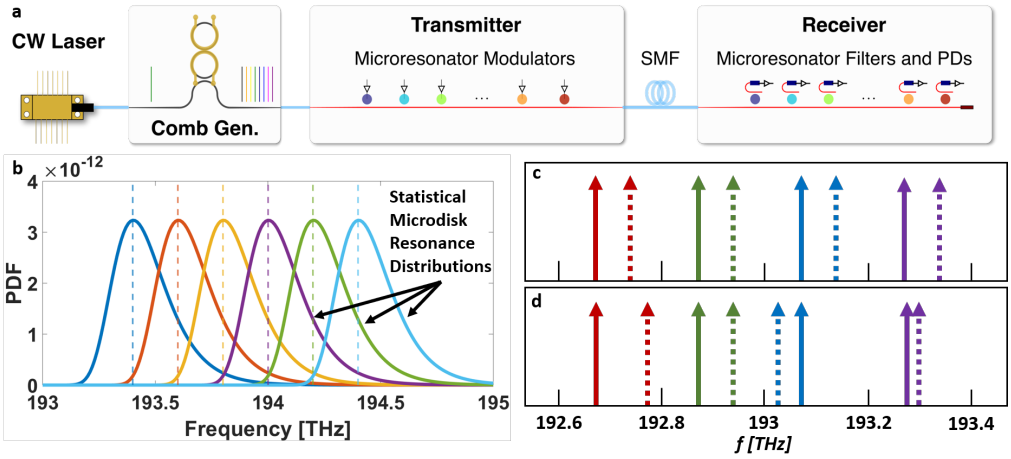

Fig. 1. a, schematic illustration of a simple Kerr-comb-based DWDM photonic link. For further discussion of the architecture, see [4]. b, illustration of the overlap of microdisk probability density functions overlaid over a 200-GHz spaced photonic transceiver optical frequency spectrum. A narrower comb, or less well-controlled device, would exhibit more severe overlap. The distributions illustrated are the measured global microdisk distributions. c, a notional four-channel optical photonic transceiver spectrum representative of those discussed in this work, albeit at reduced scale for simplification. This shows an ideal spectrum, with laser frequencies as solid arrows, and micro-resonator frequencies as dashed arrows, with no variation from designed frequencies. Operational detuning is illustrated by the displacement of the resonator frequencies from the operating laser frequencies, indicating that this is a bus that has not undergone any thermal tuning. d, the same notional architecture as c, but with one possible result of variation applied, showing how resonators may be randomly distributed in such a manner that directly tuning resonators to their intended laser frequency is forbidden. Even more extreme cases could see the frequency order of the resonators shuffled entirely out of order.

2.2. Silicon Micro-Resonators

The DWDM link architectures with high spatial density, high channel count, and low power consumption are typically implemented using microdisk, THB racetrack, and microring resonators, for both modulation of transmitted optical signals and filtering of received signals [22]. In addition to their high-speed RF modulation and filtering capabilities, these devices are also equipped with integrated resistive silicon heaters, enabling low-speed tuning of their resonant frequency [23]. For example, in microrings this can enable wide-range tuning, often across tens of nanometers, even exceeding a full FSR [24].

To compare the different types of resonators, we present data and analysis in a statistical manner, which is currently missing in the literature. In particular, the microdisk modulators under analysis consist of a 9 μm diameter silicon microdisk and a custom vertical junction for tuning. They support whispering gallery mode with an average resonant frequency of 203.005 THz. The modulators possess two RF contacts for fast encoding of electronic signals into the optical domain through free carrier dispersion effect. In addition, two low-frequency contacts for the integrated resistive thermal tuner. The THB racetrack resonators consist of two elongated parallel straight waveguide sections, which are connected at each end by a pair of 180-degree tapered bends, with an average resonant frequency of 194.606 THz. These THB resonators improve performance by reducing sidewall interaction and improving mode confinement [25].

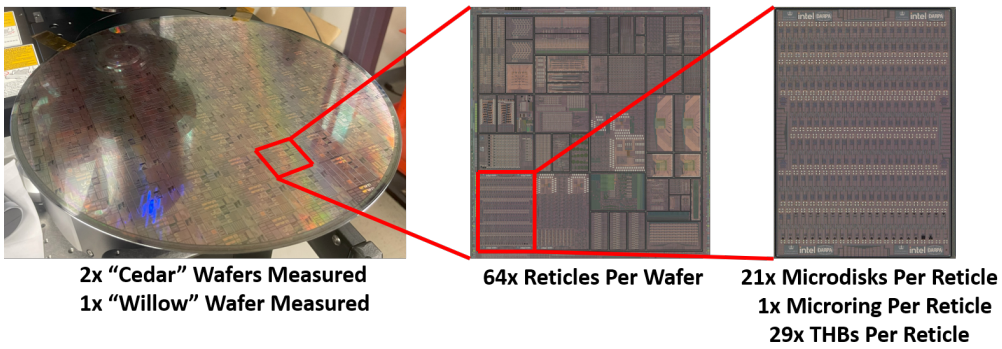

Fig. 2. Photographs and optical micrographs showing the full 300-mm custom wafer, the reticle, and the die, from which the measurement data were taken and analyzed in this work.

The microring resonators exhibit an average resonant frequency of 197.776 THz, with a similar integrated thermal tuning resistor.

We note that due to the geometrical differences between the three types of resonators, they exhibit different levels of variations. We present wafer-level characterization results for each type in the next section.

2.3. Fabrication and Measurements

We measured the three types of resonators on two iterations of our lab’s custom full-reticle 300-mm silicon photonic wafers, pictured in Fig. 2. This includes two copies of the wafer designated "Cedar" and one of the wafer designated "Willow". These wafers were fabricated by the American Institute for Manufacturing (AIM) Photonics in their silicon-on-insulator process. We measured the variation of resonant frequency, FSR, and thermal tuning efficiency using a wafer-scale test setup described below. Keysight 81068A and N7778C tunable laser sources were paired with a Keysight N7744A optical power meter to measure the optical spectra, with a Keithley 2280-32-6 high-precision DC power supply to bias the on-chip thermal phase shifters. The mass measurement of these devices was enabled via automated measurements performed by a custom ficonTEC optical wafer prober. Measurements of the microdisks involved two copies of the Cedar wafer, each with 64 nominally identical reticles. Each reticle includes 21 nominally identical microdisk modulators and 1 microring for "Cedar", and 29 nominally identical THB racetracks for "Willow". In total, we measured 2,688 microdisks, 128 microrings, and 1,856 racetracks for our variation extraction.

3. Statistics of Measured Devices

We quantify the measurement results by fitting the measured data to generalized extreme value (GEV) distributions, which can effectively capture a variety of skewing and kurtosis behaviors, while not excluding more normal distributions. The breadth of the distribution is characterized by a scale parameter σ, similar in function to the standard deviation in normal distributions. Besides this, the GEV distributions possess an additional parameter k, which describes features of the shape of the distribution, such as the general skewing behavior. The global histograms for the measured resonant frequency, along with σ and k, are given for each component in Fig. 3. We stress that existing literature is sparse about the measured fabrication variation of silicon photonic components. Most discussions rely on devices fabricated via electron beam lithography [26, 27], with limited sample sizes [28], extrapolations of resonator behavior based

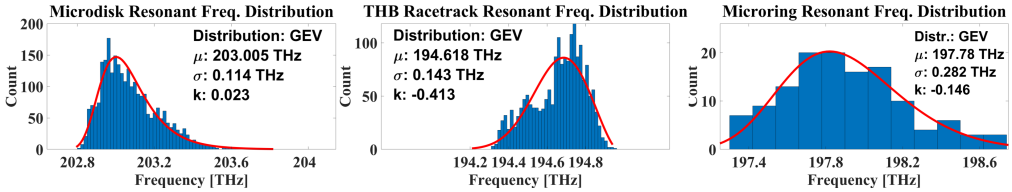

Fig. 3. Resonant frequency distributions for the measured devices, across wafer-scale measurements. The frequency axes for each plot are to-scale with each other.

on waveguide variation [17, 29], or simulation of variation of device parameters from variation of waveguides, incurring limitations in their analysis. As such, characterization of the fabrication variations on foundry-based, wafer-level silicon photonics is therefore still lacking, underlining the importance of performing such wafer-scale measurement.

The measured variation displays significant differences between the three device types. In terms of the resonant frequency distribution, microrings show a global GEV scale parameter σ of more than twice that of the microdisks, and the σ of THB racetracks is in between. The skew behavior also varies between devices. Microdisks exhibit a stronger skew than THBs, which in turn are more severely skewed than microrings. A thorough understanding of this behavior would require the measurement of many wafer copies, which is beyond the scope of this work, but some possible causes for this include variation in temperature during the measurement or, more likely, variation in some design parameter such as wafer layer thickness or dopant concentration across the wafer.

Variation considered at local and global scales differs, but is not necessarily constant in difference as spatial location changes. Significant variation exists between the scale parameters of different reticles for the microdisk, representing an interesting topic for future research. In particular, more than four-fifths of reticles achieve a microdisk scale factor σ of less than 40 GHz, nearly one-third of the global variation, which means a small number of outlier reticles significantly enlarged the global σ. We present data for both scales of variation for the microdisks. While it would be preferable to do this for the microrings as well, we do not have the required data at this time. This will, however, be sufficient to demonstrate the general principles and challenges of device and algorithm selection. For the sake of completeness, we have included the results for both reticle-wise and global distributions for the microdisks, as indicated in the respective results.

It is noteworthy that, as shown in Fig. 1b, which illustrates the global microdisk distributions, the distributions are severe compared to the channel spacing. As such, a significant portion of devices distribute outside of the designed frequency range. This behavior is quite severe in microdisks and even more substantial for microrings, with their higher variation. As the level of variation increases, the overall bus distributions become more uniform, indicating the importance of the choice of initialization algorithms. In the following section, we will discuss two types of algorithms, barrel-shifting and global-search, generally suitable for low variation and high variation, respectively.

4. Initialization Algorithms and Power Requirements

A variety of possible initialization algorithms already exist [9, 10, 22]. Here, we will consider two main types: barrel-shifting and global-search algorithms. Other names for them can be found. For example, the barrel-shifting (global-search) algorithm corresponds to a "lock to cyclic" ("lock to any") method in [10], indicating the way each algorithm works. We will discuss their principles in detail in the next section. There are also other works exploring practical implementations of thermal control algorithms for silicon photonic resonator buses [30–32].

Here, we simulate the performance for each type of algorithm using the measured statistics for each type of resonator. This study is performed by a series of Monte Carlo simulations for the two initialization algorithms to obtain the power budget required to successfully initialize at least 99.7%, or 3σ, of the simulated links. In a practical system, this will manifest as a sort of "packaging yield" or "module yield" at a given power budget, but we refer to it as the "initialization fraction". For all models, we simulated transceivers containing 16 resonators per bus. Bit-error-rate effects of non-optimal resonance alignment are not included, as prior experiments show that bit-error-free operation is readily realizable with similar micro-resonators [21].

Existing literature shows significant variation in reported values for thermal tuning efficiency values for microdisks and microrings [18, 33–38]. Moreover, we were not able to find any statistical characterization of this value in the literature. Single values were reported, but did not discuss variation of this value. As a result, while we have taken measurements of these parameters for these three devices, we cannot exhaustively state that the difference in these distributions is a deterministic result of different device geometry, as opposed to differences in a single design instance. As such, to isolate the effects of variation of the resonant frequencies and FSRs, the distribution of thermal tuning efficiency for the microdisk resonator was used for all simulations. Usage of the measured microring thermal efficiency distribution increases power consumption of ring buses by a factor of approximately 1.6, but does not affect the inter-algorithm comparison conclusions. In addition, while the distribution shapes of the respective device FSRs are used, their center values are altered to fit the appropriate FSR for a link of this design, i.e. being of a sufficient value to be greater than the overall optical bandwidth plus a small safety margin to accommodate FSR variation.

4.1. Initialization Algorithms - Barrel Shifting and Global Search

The barrel-shifting algorithm is the simplest and most robust approach, but it also suffers more difficulties under the strain of severe component variation. This approach is already discussed in detail in the literature [10, 22], but in short, an ordered bus of resonators is tuned one by one and in a fixed order to align to the laser frequencies, as shown in Fig. 4b. By forcing the frequencies of the resonators in a fixed order, the software performs the tuning in a simple step without the need for multiple iterations, hence a short tuning time. However, the resulting tuning solution is not necessarily optimal in terms of power consumption.

Global-search algorithms rely on a full search of the operating space for the initialization solution. The algorithm constructs a total map of tuning powers for each resonator, then performs a global search on this map to identify the optimal assignments of resonators to laser frequencies. This tends to achieve lower power consumption and is very robust to severe component variation. However, due to the complexity, this algorithm requires a longer execution time and potentially pre- and post-processing of the data on each end of the link to align the channels of the transmitters and receivers .

4.2. Setup of Monte Carlo Simulation

Our Monte Carlo simulation involves 10,000 modeled buses of 16-channel photonic links for each type of resonator, of which the resonant frequency, FSR, and tuning efficiency values were randomly generated from the distributions extracted from the wafer-scale measurements. A barrel-shift or global-search algorithm was applied to calculate the required initial power for the entire bus. Lastly, this process was repeated for all three types of microresonators using scaling factors from the measurement for the exact result values in Table 1, and a range of possible scale parameter values to illustrate the generalized results in Fig. 5. The fraction of links that could be initialized successfully at each possible power budget value was recorded.

4.3. Implementing the Barrel-Shifting Algorithm

A barrel-shifting algorithm seeks to initialize a link with a fixed relative order of resonators in frequency. Due to the lack of integrated coolers, in cases where multiple resonances fall between two channels, the algorithm will perform a "barrel shift" of the order by using alias resonances (resonances outside of one FSR) and shifting all resonators down in frequency by one laser frequency from their intended design frequency. Such a non-ideal case can happen as a result of large fabrication variations that shift a resonator outside of its nominal frequency range. The "barrel-shift" operation defines a new grid of resonator frequencies, including some aliasing frequencies. This process is illustrated in Fig. 4b, where two resonators are found to start between the green and blue laser frequencies. As the resonances can only be tuned the lower frequency, the blue resonator must be tuned to align with the green laser. As such, green and red resonators are aligned with red and purple, respectively. The algorithm first creates a list of frequencies, composed of the laser frequencies minus the operational detuning. Then it attempts to align the resonators to the listed frequencies in order. When a barrel-shift occurs, the resonator with the smallest resonant frequency is replaced by its alias resonance, which has one FSR higher frequency, and which now operates on the highest frequency laser line. The algorithm then realigns the lasers and resonators in order, tuning them from their "target" frequency, offset by the operational detuning, down to the actual operating laser frequency. The pseudo-code below illustrates the barrel-shifting initialization routine.

Algorithm 1 Barrel-Shifting Initialization

```
Bus ← GenerateResonatorBus()                          ▷ Generate bus of resonators from distributions.
TargetGrid ← NominalLaserGrid − OpDetuning ▷ Define TargetGrid, offset from lasers by the operational detuning
Offset ← FindWorstCaseOffset(Bus)                     ▷ Find random variation offset
VirtualGrid ← TargetGrid − Offset                     ▷ New notional grid accounts for variation
for all Resonator ∈ Bus do
    DownTune(Resonator, VirtualGrid)                  ▷ Tune each resonator down to VirtualGrid
end for
for all Resonator ∈ Bus do
    DownTune(Resonator, NominalLaserGrid) ▷ Tune entire VirtualGrid to the actual lasers
end for
```

The power can be readily calculated according to the final tuning solution found by the barrel shift algorithm. This was performed for all resonator types separately, to allow for inter-device comparison. To provide more insights into how the statistics can impact the initialization fraction, a sweep of various GEV scale parameter σ values, using microdisk distribution shapes, is presented in Fig. 5. The particular thermal power budgets required for the initialization of the various component types in the case of their actual measured global variations are given in Table 1.

4.4. Implementing the Global-Search Algorithm

Below, we describe the implementation of the global-search algorithm, which is expected to achieve low power consumption, but incur longer initialization time and additional steps to properly map electrical transmit and receive channels. The algorithm involves fully mapping the frequency operating space of each resonator, identifying all possible tuning powers corresponding to all laser frequencies. This approach is largely frequency agnostic, but with the additional hardware and complexity, it may be more challenging to implement appropriate control loops practically.

Algorithm 2 Global Search Initialization

```
Bus ← GenerateResonatorBus()                ▷ Generate bus of resonators from distributions.
TargetGrid ← NominalLaserGrid − OpDetuning  ▷ Define TargetGrid, offset from lasers by the operational detuning
for all Resonator ∈ Bus do
    Detune(Resonator)                       ▷ Move resonators out of the operating band.
    Spectrum(Resonator) ← SweepResonator(Resonator, TargetGrid)   ▷ Sweep each resonator, one at a time, across the operating band, recording which tuning powers correspond to peak received power.
end for
MappingTable ← AssembleMappingTable(Spectrum)   ▷ Compute a map of all tuning powers required to tune all resonators to all lasers.
Assignments ← LinearSolution(MappingTable)      ▷ Find the linear solution of the MappingTable matrix
DownTune(Bus, Assignments)                  ▷ Tune resonators down to their assigned lasers
```

Our implementation of the global-search algorithm is summarized as follows. First, all resonators are blue-shifted out of the main operating band of the bus. Then, each resonator is thermally tuned across the entire band and the optical power at each step is recorded. In experiments, such a detection may be implemented through various means, such as local photodiodes for each resonator or a common photodiode at the end of bus. Either the primary design resonant frequency or one of its aliases can be used and are treated as equally valid assignments to ensure that all resonators can be tuned to every possible laser frequency. Once this has been completed for all resonators, a full tuning power-optical power map is constructed, according to which the resonators are aligned to the laser frequencies such that the total power consumption is minimized. We note that this optimization problem is a classic balanced linear assignment problem, and can be solved via a typical linear program. We assume no extra constraints while aligning the resonator to the laser frequencies. However, in reality, there may exist a maximum allowed power, due to limited driver circuitry or maximum thermal tuning power limits. Such a limitation could be introduced and would possibly increase the total initialization power or reduce typical module bandwidth, depending on the nature of the limitation imposed and component variation. The identified tuning powers may then be applied to each resonator, along with power sufficient to account for the operational detuning, to complete the initialization. This process is illustrated in Fig. 4. The particular thermal power budgets required for the initialization of the various component types are given in Table 1, and a generalized sweep of a range of GEV scale parameters in Fig. 5.

5. Time Dependent Behavior

The relevance of initialization time is highly dependent on the intended application. For datacenter applications, under certain computational loads, a pre-heating phase can be used to bring the photonic components up to a nearly static operating temperature, and as long as the components remain within a temperature range of a few degrees Celsius, no repeat initializations will be required. In this case, the re-initialization time will be largely irrelevant. If, however, such a pre-heat phase is not possible, or if large and fast fluctuations in temperature occur, re-initialization will be required any time the temperature is outside the limits of the operational detuning. In such a case, the initialization time may be of significant concern to the system designers. Any re-initialization during link operations will increase energy per bit and reduce average bandwidth from nominal values. A brief discussion of such effects based on known thermal properties is presented. This discussion is valuable for applications where the initial start-up time is of

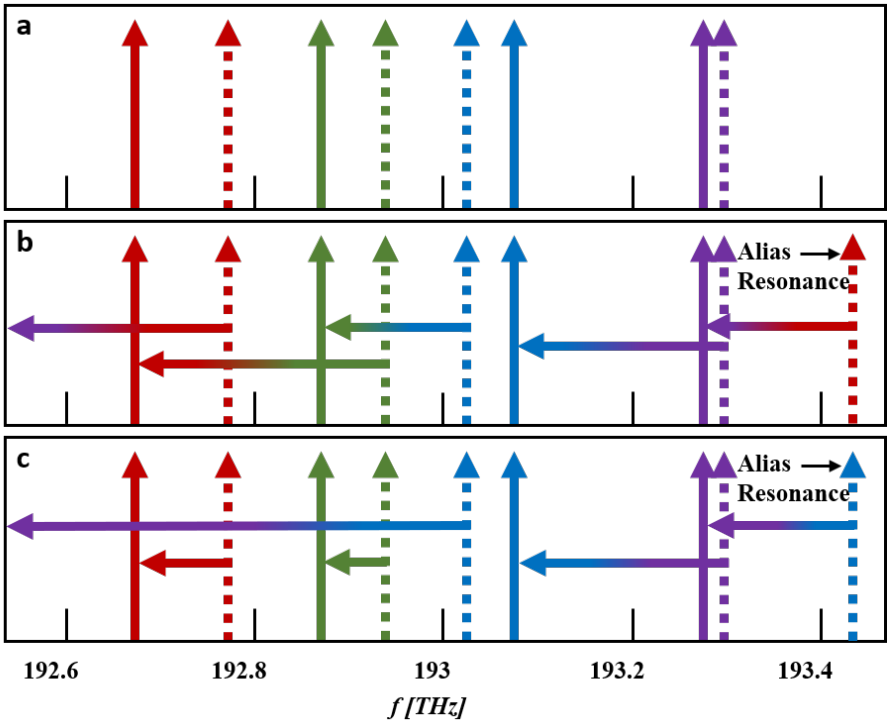

Fig. 4. Schematic illustration of the resulting assignments of the two initialization algorithms. In a, we see the spectrum of a notional bus of fabricated resonators with a realistic degree of variation applied, with laser frequencies in solid lines and resonator frequencies in dotted lines. In b, the resultant assignment of the barrel-shift initialization, with horizontal arrows indicating tuning performed to reach the alignment and gradient arrows indicating the reassignment of resonators from their original, intended laser frequencies. In c, similar to b, but with the implementation of the global-search algorithm.

concern or where frequent system reconfigurations are required.

The precise time required to re-initialize a link will be implementation and hardware-specific, although an interesting approximation may be made through a specific quality of the heaters used for tuning: as a thermal component, they possess a thermal time constant which, by the standards of most electronic control loops, is quite slow. Again, this value will vary depending on component geometry, but typically presents a bandwidth of approximately 10-100 kHz. In a prior link experiment [21], we found that one instance of our microring filters required a 10 μs delay immediately following any assignment of a voltage to the heater by writing to a DAC, to allow for the resonator to settle at its newly tuned frequency. This, in our case, dominated the total time required for tuning, as relatively few instructions had to be executed for each DAC write, and those instructions were largely not mathematically intensive. This value also represented a floor, as determined heuristically. As such, we can estimate the required initialization time for these two algorithm families based on the number of DAC writes and the 10 μs DAC write time.

The barrel shifting algorithm is relatively simple to initialize during actual operations if the link is well characterized. When the temperature shift becomes sufficiently severe as to force resonators out of the operational range of a given initialization, the resonator assignments are simply barrel shifted down in frequency to the next laser line in their fixed order, similar to the

barrel shifting sometimes required during initialization. A few DAC writes may be needed to find the precise tuning value for the next laser frequency, but not likely more than a small handful, perhaps a dozen at most. Parallelization is algorithmically possible, and strongly recommended for larger buses, as it will reduce initialization time down to the value for a single resonator, as opposed to multiplying the time by the resonator count. In such a case, this limits the required time to a channel-count independent value of, to an order of magnitude, 100 μs. This is also insensitive to total channel count.

The global-search initialization process is more involved and much more lengthy, as well as highly channel-count dependent, primarily due to the measurement phase where the assignment map is constructed. Each resonator must be swept across the entire operating frequency band, one at a time, at a hardware-dependent step size and in a manner which is hostile to parallelization - while it may be possible, it is not nearly as intuitive or simple as the barrel shifting approach, and would require great care. We can consider one case based off the generic bus architecture modeled above, with sixteen resonators at a 200 GHz spacing, and with a step size of half a resonator's full-width half max, or about 15 GHz, this would present a required DAC write count of approximately 213 per resonator (rounded), or 3,408 total assuming no parallelization. This, while likely a moderate underestimate, translates to an initialization time of 34,080 μs, or 340.8 times as long as the barrel shifting re-initialization. More generically, this approximation can be given as:

$$t_{reinit} = t_{DACwrite} n_{res}^2 f_{comb} f_{HWHM}^{-1}$$

The re-initialization time, then, has a linear dependency on the time to perform a DAC write, itself determined by the thermal bandwidth of the resonator, the laser frequency comb spacing, and the resonance width. More importantly, the re-initialization time scales with the square of the resonator count per-bus, providing a good motivation for the development of interleaver systems to allow for bus parallelization. If the hardware, compute load, or link architecture required frequent re-initialization, this could constitute a serious problem, potentially reducing average bandwidth by a noticeable fraction, and imposing higher energy costs per bit than might otherwise be expected. The barrel shifting algorithm can mitigate this issue through speed, although for maximally optimized links, we believe a global-search initialization paired with a system pre-heat phase will typically produce superior performance when low variation components are available.

6. Analysis and Further Discussion

The results presented above demonstrate the challenges inherent to the co-analysis of the initialization fraction and variation of micro-resonator-based silicon photonic transceivers. We can, however, draw several conclusions relevant to our goal of high initialization fraction, low-power silicon photonic transceivers.

	Barrel Shift	**Global Search**
Microring	556 mW	231 mW
THB Racetrack	277 mW	182 mW
Microdisk	123 mW	104 mW
Init. Time	0.1 ms	34 ms

Table 1. Power required to initialize more than 99.7% (3σ yield) of simulated resonator buses under differing variations and initialization algorithms. These values are for the global variation scale parameters for the respective devices. Other values may be gleaned from the generalized gradient plots in Fig. 5.

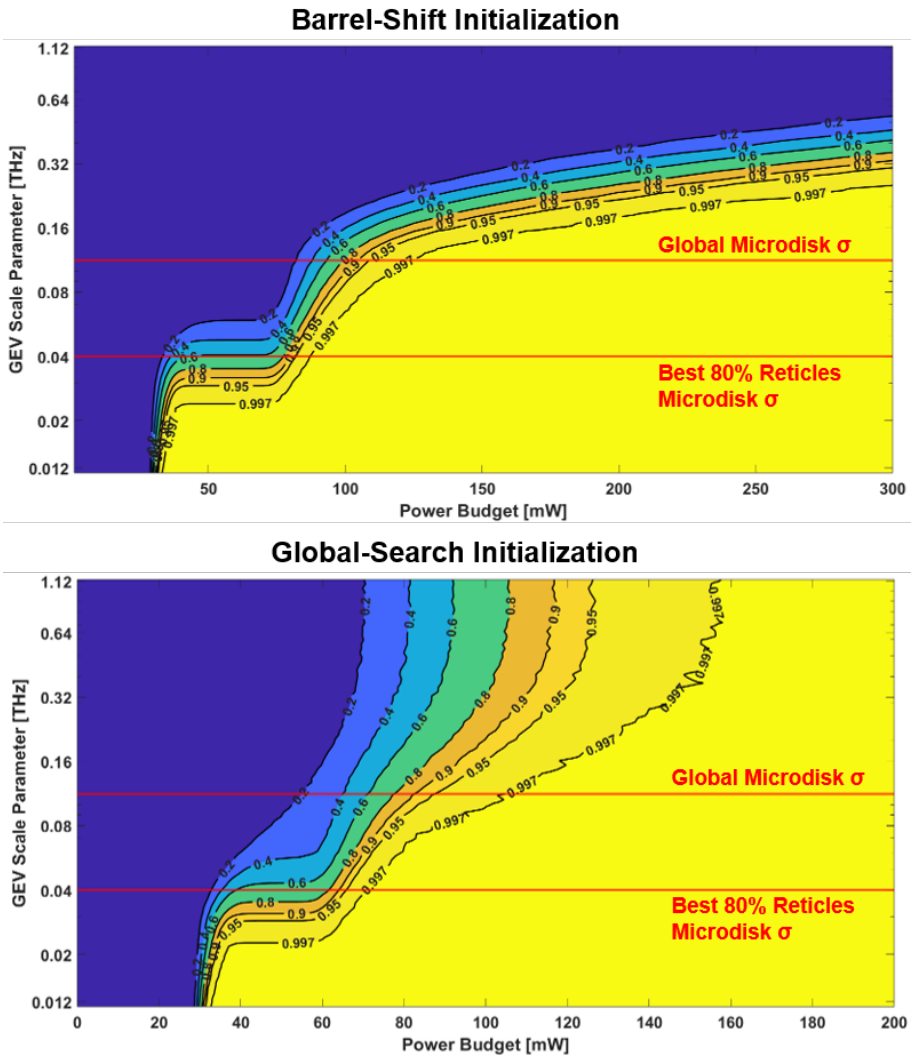

Fig. 5. Generalized gradient plot of the initialization fraction of 10,000 modeled buses for each initialization algorithm. The plots illustrate the required power budget to initialize various fractions of the generated buses at different possible scale parameters for the microdisk distribution shapes. Also illustrated are the global microdisk scale parameter and the local scale parameter for the best 80% of reticles.

Figure 5, top, shows that barrel-shifting algorithms demonstrate a strong initialization fraction-power budget dependence on the variation of the resonant frequency of the fabricated resonator. For low-variation components, the initialization power budget for a given initialization fraction is similar to that of the global-search initialization algorithm. However, as variation increases, required power budget to maintain that initialization fraction increases dramatically and non-linearly, due to the offset defined by the most severely varied component. The "leap" in power budget observed between 20 and 60 GHz can be attributed to the range where we first observe a requirement for an initial barrel-shift, as this then imposes a shift down in frequency equal to the comb spacing on every resonator on the bus, plus some additional shift to use the alias resonance of the lowest frequency resonator. It should be concluded that, for high variation components, barrel-shifting cannot be recommended for low-power initializations.

Figure 5, bottom, indicates that global-search initialization algorithms exhibit a strong resilience to fabrication variation, even at higher initialization fraction rates. In our simulations, global-search algorithms allow a much more variation-tolerant route to low-power initialization compared to the barrel shifting algorithm. While global-search initializations require additional data pre- and post-processing to properly map electrical signals at the transmitter and receiver end, and require longer initialization times, they may be non-optional if variation cannot be reduced in fabrication. Reducing variation in production will likely be challenging, as electronic circuit fabrication often sees very high absolute parameter variation, even in much more mature processes. While exact values vary, for similar processes to those used in silicon photonic fabrication, key geometric parameters can vary by more than 25% [39]. The relatively large size of silicon photonic resonators, compared to transistors, will reduce the ability of designers to rely on proximity-based component matching, as resonators on a bus may be displaced from each other by a millimeter or more in a practical system, and a relatively large minimum separation must be maintained to avoid thermal crosstalk between thermally tuned resonators. The "leap" here is less clear, and varies more between the different gradients, with the initial "leap" indicating the minimum scale parameter to require some significant shuffling of the resonators.

The improvements in power budget are clear at the 3σ initialization fraction level. We first compare the power and time under the global variation values for each component type. A bus of microdisks using the barrel-shifting method would require 123 mW, while global search would require 104 mW, representing a modest reduction. For microrings, barrel-shifting would require 556 mW, while global-search only requires 231 mW, showing a substantial reduction of more than 2.4×. For THBs, the improvement from 277 mW to 182 mW represents a reduction of 1.5×. Clearly, for links demanding high-initialization fraction and with high variation, global-search initialization is necessary to achieve low maximum power budgets, but for low variation devices, the small additional power consumption of the barrel-shifting initialization may be justified by the dramatically superior speed.

7. Conclusion

We have presented wafer-scale statistical measurements of over 4,600 silicon photonic resonators, including microdisks, THB racetracks, and microrings, and analyzed their impact on DWDM link initialization. Monte Carlo simulations using these distributions show that barrel-shifting enables fast, sub-millisecond initialization with modest power for low-variation devices such as microdisks, but becomes power-inefficient for higher-variation devices. In contrast, global-search achieves substantially lower power consumption and robust initialization for high-variation devices such as microrings, albeit with about 300× longer runtime. THB racetracks exhibit intermediate behavior. These results establish a quantitative framework linking fabrication variation to initialization performance, providing practical guidance for selecting algorithms that balance speed, power, and yield in silicon photonic DWDM interconnects.

Funding

This work was supported in part under the SMART Scholarship Program, funded by the OUSD/R&E (The Under Secretary of Defense-Research and Engineering), National Defense Education Program (NDEP) / BA-1, Basic Research. This work was also supported in part by the Center for Ubiquitous Connectivity (CUbiC), sponsored by Semiconductor Research Corporation (SRC) under award number (SRC 2023-JU-3132) and Defense Advanced Research Projects Agency (DARPA) under the JUMP 2.0 program and award number (HR0011-23-3-0002).

Disclosures

The authors declare no conflicts of interest.

Data Availability

Data underlying the results presented in this paper are not publicly available at this time but may be obtained from the authors upon reasonable request.

References

1. D. A. B. Miller, "Attojoule optoelectronics for low-energy information processing and communications," J. Light. Technol. **35**, 346–396 (2017).
2. M. Wade, E. Anderson, S. Ardalan, *et al.*, "Teraphy: A chiplet technology for low-power, high-bandwidth in-package optical i/o," IEEE Micro **40**, 63–71 (2020).
3. M. Khani, M. Ghobadi, M. Alizadeh, *et al.*, "Sip-ml: high-bandwidth optical network interconnects for machine learning training," in *Proceedings of the 2021 ACM SIGCOMM 2021 Conference,* (Association for Computing Machinery, New York, NY, USA, 2021), SIGCOMM '21, p. 657–675.
4. A. Rizzo, A. Novick, V. Gopal, *et al.*, "Massively scalable kerr comb-driven silicon photonic link," Nat. Photonics **17**, 781–790 (2023).
5. J. Chen, W. Wei, J. Qin, *et al.*, "8×100gbps o-band dwdm transmitter empowered by comb laser and micro-ring modulator array for optical interconnects," in *2024 IEEE 29th International Semiconductor Laser Conference (ISLC),* (2024), pp. 1–2.
6. P.-H. Chang, A. Samanta, P. Yan, *et al.*, "A 3d integrated energy-efficient transceiver realized by direct bond interconnect of co-designed 12 nm finfet and silicon photonic integrated circuits," J. Light. Technol. **41**, 6741–6755 (2023).
7. M. Nikdast, G. Nicolescu, J. Trajkovic, and O. Liboiron-Ladouceur, "Chip-scale silicon photonic interconnects: A formal study on fabrication non-uniformity," J. Light. Technol. **34**, 3682–3695 (2016).
8. W. Bogaerts, Y. Xing, and U. Khan, "Layout-aware variability analysis, yield prediction, and optimization in photonic integrated circuits," IEEE J. Sel. Top. Quantum Electron. **25**, 1–13 (2019).
9. M. Hattink, Z. Zhu, and K. Bergman, "Automated tuning and channel selection for cascaded micro-ring resonators," in *Metro and Data Center Optical Networks and Short-Reach Links III,* vol. 11308 A. K. Srivastava, M. Glick, and Y. Akasaka, eds., International Society for Optics and Photonics (SPIE, 2020), p. 113080P.
10. S. Choi and V. Stojanović, "Scalable wavelength arbitration for microring-based dwdm transceivers," J. Light. Technol. **43**, 5100–5116 (2025).
11. S. Pasricha and M. Nikdast, "A survey of silicon photonics for energy-efficient manycore computing," IEEE Des. & Test **37**, 60–81 (2020).
12. B. G. Lee, N. Nedovic, T. H. Greer, and C. T. Gray, "Beyond cpo: A motivation and approach for bringing optics onto the silicon interposer," J. Light. Technol. **41**, 1152–1162 (2023).
13. S. Fathololoumi, C. Malouin, D. Hui, *et al.*, "Highly integrated 4 tbps silicon photonic ic for compute fabric connectivity," in *2022 IEEE Symposium on High-Performance Interconnects (HOTI),* (2022), pp. 1–4.
14. Y. Okawachi, B. Y. Kim, M. Lipson, and A. L. Gaeta, "Chip-scale frequency combs for data communications in computing systems," Optica **10**, 977–995 (2023).
15. W. A. Zortman, D. C. Trotter, and M. R. Watts, "Silicon photonics manufacturing," Opt. Express **18**, 23598–23607 (2010).
16. H. Jayatilleka, H. Frish, R. Kumar, *et al.*, "Post-fabrication trimming of silicon photonic ring resonators at wafer-scale," J. Light. Technol. **39**, 5083–5088 (2021).
17. Z. Lu, J. Jhoja, J. Klein, *et al.*, "Performance prediction for silicon photonics integrated circuits with layout-dependent correlated manufacturing variability," Opt. Express **25**, 9712–9733 (2017).
18. F. Gan, T. Barwicz, M. A. Popovic, *et al.*, "Maximizing the thermo-optic tuning range of silicon photonic structures," in *2007 Photonics in Switching,* (2007), pp. 67–68.
19. R. Amatya, C. Holzwarth, H. Smith, and R. J. Ram, "Efficient thermal tuning for second-order silicon nitride microring resonators," in *2007 Photonics in Switching,* (2007), pp. 149–150.
20. R. Amatya, C. Holzwarth, M. A. Popovic, *et al.*, "Low power thermal tuning of second-order microring resonators," in *2007 Conference on Lasers and Electro-Optics (CLEO),* (2007), pp. 1–2.
21. M. Hattink, J. Robinson, L. Y. Dai, *et al.*, "Wide temperature range uncooled 2.5d integrated silicon photonic dwdm receiver," in *2024 Goverment Microcircuit Applications & Critical Technology Conference,* (2024).
22. Y. Wang, A. Novick, R. Parsons, *et al.*, "Scalable architecture for sub-pJ/b multi-Tbps comb-driven DWDM silicon photonic transceiver," in *Next-Generation Optical Communication: Components, Sub-Systems, and Systems XII,* vol. 12429 G. Li, K. Nakajima, and A. K. Srivastava, eds., International Society for Optics and Photonics (SPIE, 2023), p. 124291F.
23. A. Novick, S. Wang, A. Rizzo, *et al.*, "Ultra-efficient interleaved vertical-junction microdisk modulator with integrated heater," in *2024 Optical Fiber Communications Conference and Exhibition (OFC),* (2024), pp. 1–3.
24. J. Sun, R. Kumar, M. Sakib, *et al.*, "A 128 gb/s pam4 silicon microring modulator with integrated thermo-optic resonance tuning," J. Light. Technol. **37**, 110–115 (2019).
25. K. Jang, A. Novick, R. Parsons, and K. Bergman, "Tapered-hybrid bend, interior-ridge modulator and filter supporting tbps-scale links," in *2025 Optical Fiber Communications Conference and Exhibition (OFC),* (2025), pp. 1–3.
26. M. Nikdast, G. Nicolescu, J. Trajkovic, and O. Liboiron-Ladouceur, "Photonic integrated circuits: A study on process variations," in *2016 Optical Fiber Communications Conference and Exhibition (OFC),* (2016), pp. 1–3.
27. A. Mirza, R. E. Gloekler, S. Pasricha, and M. Nikdast, "Provat: An automated design and analysis framework for process-variation-resilient design of silicon photonic microring resonators," IEEE Trans. on Comput. Des. Integr. Circuits Syst. pp. 1–1 (2024).
28. A. Mirza, S. Pasricha, and M. Nikdast, "Variation-aware inter-device matching in silicon photonic microring resonator

demultiplexers," in *2020 IEEE Photonics Conference (IPC),* (2020), pp. 1–2.
29. X. Cao, S. Bhatnagar, M. Nikdast, and S. Roy, "Hierarchical polynomial chaos for variation analysis of silicon photonics microresonators," in *2019 International Applied Computational Electromagnetics Society Symposium (ACES),* (2019), pp. 1–2.
30. P. Dong, R. Gatdula, K. Kim, *et al.*, "Simultaneous wavelength locking of microring modulator array with a single monitoring signal," Opt. Express **25**, 16040–16046 (2017).
31. H.-K. Kim, J.-H. Lee, M. Kim, *et al.*, "A 4-λ × 28-gb/s/λ silicon ring-resonator-based wdm receiver with a reconfigurable temperature controller," J. Light. Technol. **42**, 2296–2302 (2024).
32. Z. Wang, D. Ming, Y. Wang, *et al.*, "An electronic-photonic converged adaptive-tuning-step pipelined time-division-multiplexing control scheme for fast and scalable wavelength locking of micro-rings," J. Light. Technol. **40**, 5622–5630 (2022).
33. C. Sun, M. Wade, M. Georgas, *et al.*, "A 45 nm cmos-soi monolithic photonics platform with bit-statistics-based resonant microring thermal tuning," IEEE J. Solid-State Circuits **51**, 893–907 (2016).
34. Q. Deng, A. H. El-Saeed, A. Elshazly, *et al.*, "32×100 ghz wdm filter based on ultra-compact silicon rings with a high thermal tuning efficiency of 5.85 mw/pi," in *2024 Optical Fiber Communications Conference and Exhibition (OFC),* (2024), pp. 1–3.
35. D. Coenen, H. Oprins, Y. Ban, *et al.*, "Thermal modelling of silicon photonic ring modulator with substrate undercut," J. Light. Technol. **40**, 4357–4363 (2022).
36. R. Parsons, A. Novick, M. Hattink, *et al.*, "Efficient silicon photonic add-drop microdisk filters for dwdm systems," in *2023 Conference on Lasers and Electro-Optics (CLEO),* (2023), pp. 1–2.
37. N. J. D. Martinez, C. T. Derose, R. Jarecki, *et al.*, "Low power thermal tuning in resonant vertical junction silicon modulators through substrate removal," IEEE Photonics J. **10**, 1–12 (2018).
38. A. Rizzo, V. Deenadayalan, M. v. Niekerk, *et al.*, "Ultra-efficient foundry-fabricated resonant modulators with thermal undercut," in *2023 Conference on Lasers and Electro-Optics (CLEO),* (2023), pp. 1–2.
39. A. Chandrakasan, W. J. Bowhill, and F. Fox, *Models of Process Variations in Device and Interconnect* (Wiley-IEEE Press, 2001), pp. 98–115.